molecules

MDPI

Article

Thiourea-Derived Chelating Ligands and Their Organometallic Compounds: Investigations into Their Anticancer Inhibitory Activity

Kelvin K.H. Tong [1], Muhammad Hanif [1], James H. Lovett [2], Katja Hummitzsch [3], Hugh H. Harris [2], Tilo Söhnel [1], Stephen M. F. Jamieson [4] and Christian G. Hartinger [1,*]

[1] School of Chemical Sciences, University of Auckland, Private Bag 92019, Auckland 1142, New Zealand
[2] Department of Chemistry, The University of Adelaide, Adelaide, 5005 SA, Australia
[3] Discipline of Obstetrics and Gynecology, The University of Adelaide, Robinson Research Institute, Adelaide, 5005 SA, Australia
[4] Auckland Cancer Society Research Centre, University of Auckland, Private Bag 92019, Auckland 1142, New Zealand
* Correspondence: c.hartinger@auckland.ac.nz; Tel.: +64-9-3737599 83220 (C.G.H.); web: http://hartinger.auckland.ac.nz/

Received: date; Accepted: date; Published: date

Table of Contents

Table S1. ESI-MS data for compounds **a**, **b**, **1a**-**4b**, **1a**^{Cl}-**4b**^{Cl} and **1b**^{NH3} analyzed in positive ion mode.

Compound	Observed *m*/*z*	Theoretical *m*/*z*	Assignment
a	358.1106	358.1102	$[M + Na]^+$
b	308.0942	308.0946	$[M + Na]^+$
1a	606.1034	606.1032	$[M – PF_6]^+$
1a^{Cl}	606.1024	606.1032	$[M – Cl]^+$
2a	696.1576	696.1603	$[M – PF_6]^+$
2a^{Cl}	696.1576	696.1603	$[M – Cl]^+$
3a	608.1125	608.1122	$[M – PF_6]^+$
3a^{Cl}	574.1487	574.1506	$[M – 2Cl – H]^+$
4a	698.1672	698.1696	$[M – PF_6]^+$
4a^{Cl}	662.1949	662.1929	$[M – 2Cl – H]^+$
1b	556.0836	556.0876	$[M – PF_6]^+$
1b^{Cl}	556.0871	556.0876	$[M – Cl]^+$
1b^{NH3}	683.1120	683.1094	$[M – PF_6]^+$
2b	646.1422	646.1447	$[M – PF_6]^+$
2b^{Cl}	646.1422	646.1447	$[M – Cl]^+$
3b	524.1357	524.1324	$[M – Cl – PF_6 – 3H + 2D]^+$
3b^{Cl}	524.1338	524.1324	$[M – 2Cl – 3H + 2D]^+$
4b	612.1848	612.1769	$[M – Cl – PF_6 – H]^+$
4b^{Cl}	612.1778	612.1773	$[M – 2Cl – H]^+$

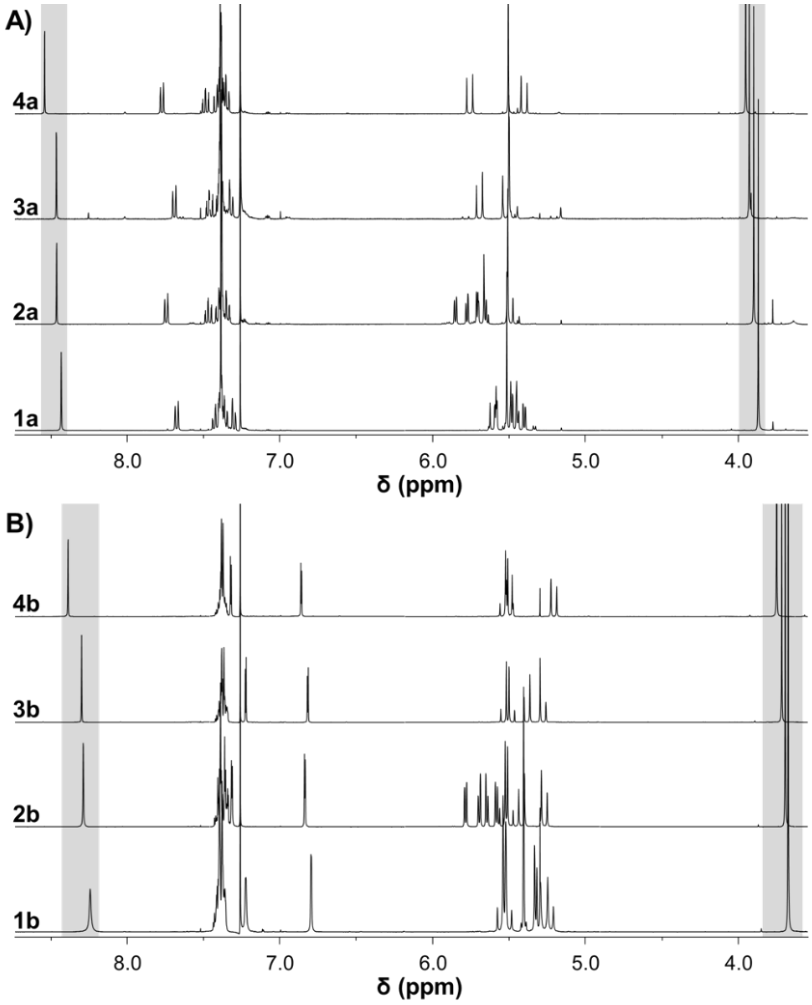

Figure S1. Comparison of the ^{1}H NMR spectra of complexes **1a**-**4a** (A) and **1b**–**4b** (B). The triazole and methyl H peaks shifting in dependence of the metal center are highlighted with grey boxes.

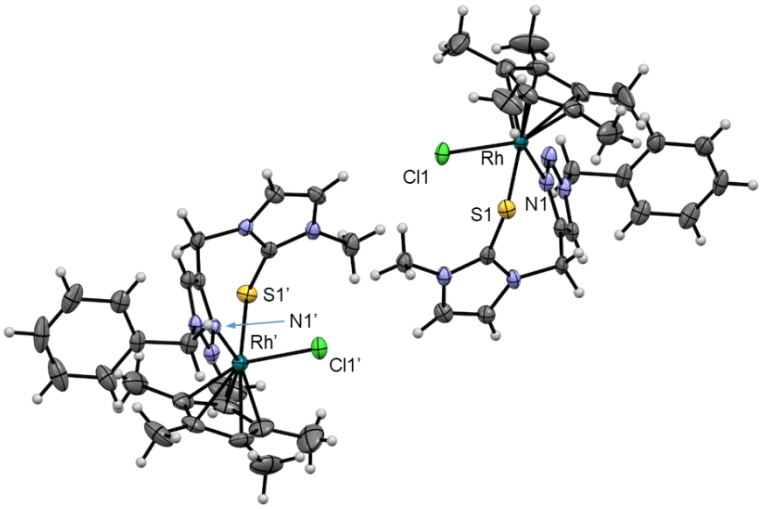

Figure S2. Molecular structures of the two enantiomers of **3b**. Counterions have been omitted for clarity and the structures are shown at 50% probability level.

Table S2. X-ray crystallographic data for complex **1b**^{NH3}, **2a**, **2a**^{Cl}, **3b**, **3b**^{Cl}, **4a**, and **4b**^{Cl}.

	1b^{NH3}	**2a**^{Cl}·H_2O	**3b**·toluene	**3b**^{Cl}·H_2O·toluene	**4a**·$CHCl_3$	**4b**^{Cl}·H_2O
CCDC	2013780	2013781	2013782	2013783	2013784	2013785
Formula	$C_{24}H_{32}N_6RuSP_2F_{12}$	$C_{28}H_{31}Cl_2N_5OsS$·2.25H_2O	$C_{24}H_{30}ClN_5RhSPF_6$·0.5C_7H_8 [+H_2O]#	$C_{24}H_{30}Cl_2N_5RhS$·1.5H_2O [+ C_7H_8 + H_2O]#	$C_{28}H_{32}ClIrN_5SPF_6$·3$CHCl_3$	$C_{24}H_{30}Cl_2IrN_5S$·1.25H_2O
Formula weight [g mol^{-1}]	827.62	771.27	749.98	621.42	1201.37	706.21
Temperature [K]	99.8(3)	100.0(1)	100.0(2)	100.0(1)	100.0(1)	100.0(1)
Crystal System	monoclinic	monoclinic	orthorhombic	triclinic	monoclinic	triclinic
Space group	$P2_1/n$	$P2_1/n$	$Pna2_1$	P-1	$P2_1/c$	P-1
***a* [Å]**	9.06730(9)	10.77920(10)	29.9478(3)	8.49050(10)	12.49577(7)	8.3119(2)
***b* [Å]**	12.95883(13)	9.14240(10)	8.43080(10)	18.6371(2)	11.25335(6)	18.9967(3)
***c* [Å]**	27.5090(2)	29.8464(3)	25.6410(3)	19.1728(2)	32.00737(18)	19.2510(3)
α [º]	90	90	90	96.503(1)	90	62.526(1)
β [º]	97.9021(9)	90.727(1)	90	90.247(1)	94.3484(5)	85.408(1)
γ [º]	90	90	90	94.121(1)	90	80.034(1)
***V* [Å^3]**	3201.66(5)	2941.06(5)	6473.94(13)	3006.32(6)	4487.90(4)	2656.20(9)
Z	4	4	8	4	4	4
ϱ_{calc} [g/cm^3]	1.717	1.742	1.539	1.478	1.778	1.766
μ [mm^{-1}]	6.424	10.818	6.640	7.124	12.506	12.540
F(000)	1664.0	1530.0	3048.0	1378.0	2352.0	1394.0
Crystal size [mm^3]	0.10 × 0.10 × 0.05	0.08 × 0.08 × 0.01	0.05 × 0.05 × 0.01	0.20 × 0.12 × 0.08	0.12 × 0.10 × 0.05	0.50 × 0.01 × 0.01
2Θ range for data collection [°]	11.898 to 135.472	11.35 to 135.454	11.436 to 136.492	11.174 to 135.476	11.086 to 136.496	11.362 to 136.482
Index ranges	$-10 \le h \le 10$, $-15 \le k \le 15$, $-28 \le l \le 32$	$-12 \le h \le 12$, $-10 \le k \le 10$, $-35 \le l \le 35$	$-36 \le h \le 33$ $-7 \le k \le 10$, $-30 \le l \le 30$	$-10 \le h \le 10$, $-22 \le k \le 20$, $-23 \le l \le 23$	$-15 \le h \le 14$, $-13 \le k \le 13$, $-38 \le l \le 38$	$-10 \le h \le 10$, $-22 \le k \le 22$, $-23 \le l \le 23$

Table S2. contd.

	1b^{NH3}	**2a**^{Cl}·H_2O	**3b**·toluene	**3b**^{Cl}·H_2O·toluene	**4a**·$CHCl_3$	**4b**^{Cl}·H_2O
Reflections collected	44752	36743	50594	95171	71288	79200
Independent reflections	5785 [R_{int} = 0.0399, R_{sigma} = 0.0213]	5300 [R_{int} = 0.0379, R_{sigma} = 0.0216]	11382 [R_{int} = 0.0354, R_{sigma} = 0.0317]	10870 [R_{int} = 0.0725, R_{sigma} = 0.0357]	8213 [R_{int} = 0.0506, R_{sigma} = 0.0242]	9686 [R_{int} = 0.0593, R_{sigma} = 0.0278]
Data / restraints / parameters	5785 / 42 / 486	5300 / 0 / 396	11382 / 53 / 779	10870 / 0 / 671	8213 / 4 / 530	9686 / 0 / 658
Goodness-of-fit on F^2	1.032	1.056	1.032	1.054	1.060	1.105
Final R indexes [I>=2σ (I)]	R_1 = 0.0210	R_1 = 0.0186	R_1 = 0.0327	R_1 = 0.0372	R_1 = 0.0300	R_1 = 0.0372
	wR_2 = 0.0502	wR_2 = 0.0450	wR_2 = 0.0838	wR_2 = 0.0991	wR_2 = 0.0718	wR_2 = 0.0923
Final R indexes [all data]	R_1 = 0.0220	R_1 = 0.0205	R_1 = 0.0349	R_1 = 0.0420	R_1 = 0.0308	R_1 = 0.0414
	wR_2 = 0.0507	wR_2 = 0.0458	wR_2 = 0.0852	wR_2 = 0.1026	wR_2 = 0.0725	wR_2 = 0.0947
Largest diff. peak / hole [e $Å^{-3}$]	0.34 / -0.39	0.80 / -0.66	0.78 / -0.53	0.86 / -1.18	1.67 / -1.11	2.31 / -2.27
Flack parameter	-	-	-0.011(4)	-	-	-

[#] Highly disordered solvent; excluded with solvent mask from final refinements

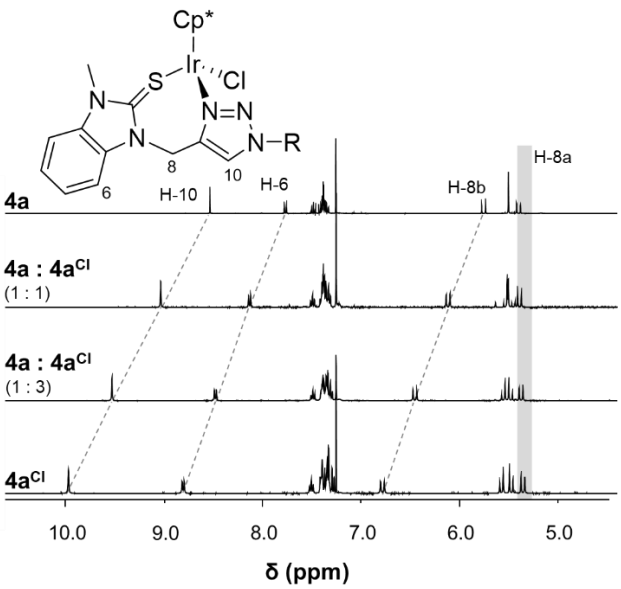

Figure S3. The aromatic regions of the ^{1}H NMR spectra of **4a** with its PF_6^- counterion and the chloride derivative **4a**^{Cl} and both compounds mixed at 1 : 1 and 1 : 3 ratios, recorded in $CDCl_3$.

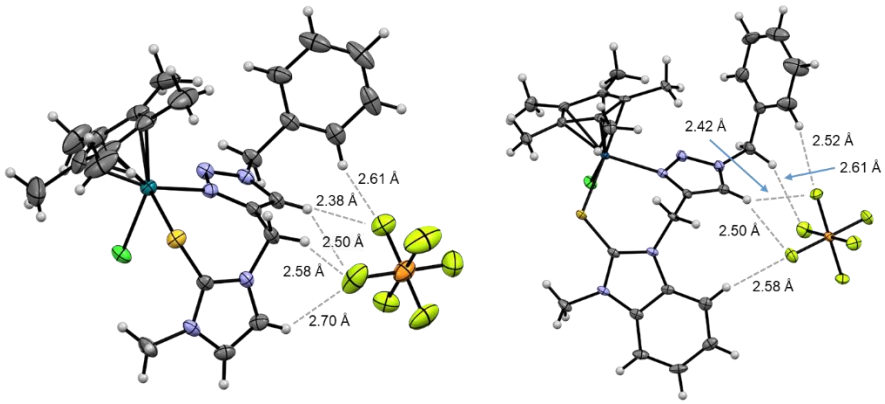

Figure S4. Interactions between the PF_6^- counterions and the complex cations in **3b** (left) and **4a** (right) with the C–H···F distances shown. Co-crystallized solvent molecules have been omitted for clarity and the structures are drawn at 50% probability level.

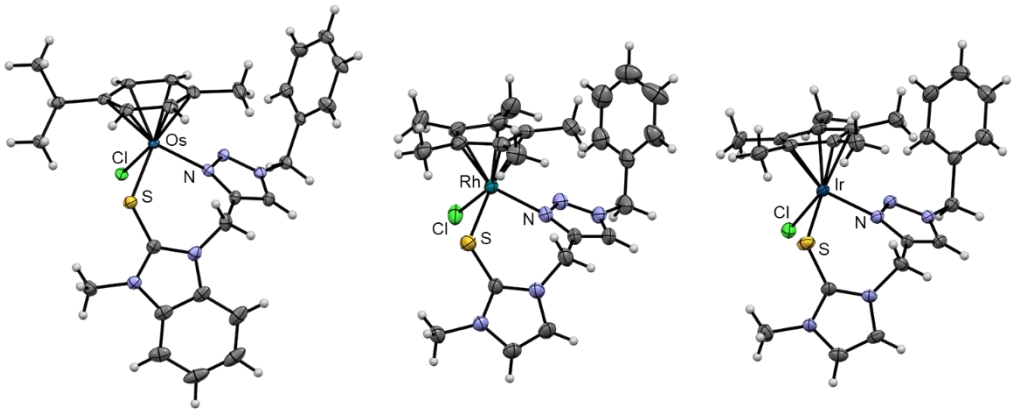

Figure S5. Molecular structures of one of the enantiomers found for **2a**^{Cl}, **3b**^{Cl}, and **4b**^{Cl}. Counterions and co-crystallized solvent molecules have been omitted for clarity and the structures are drawn at 50% probability level.

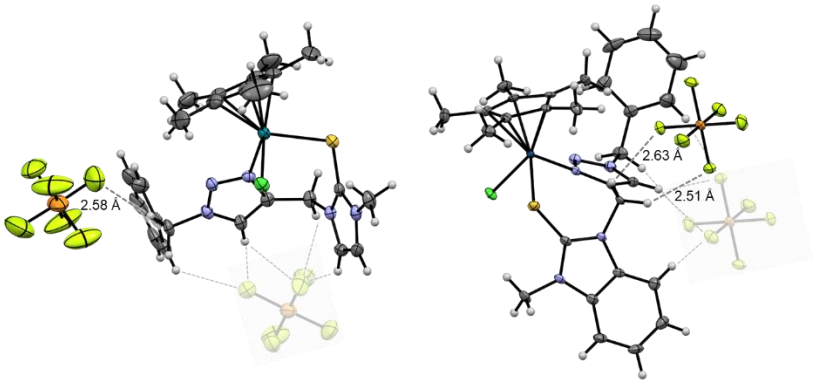

Figure S6. Secondary interactions between the PF_6^- counterions and the complex cations in **3b** (left) and **4a** (right). Co-crystallized solvent molecules have been omitted for clarity and the structures are drawn at 50% probability level.

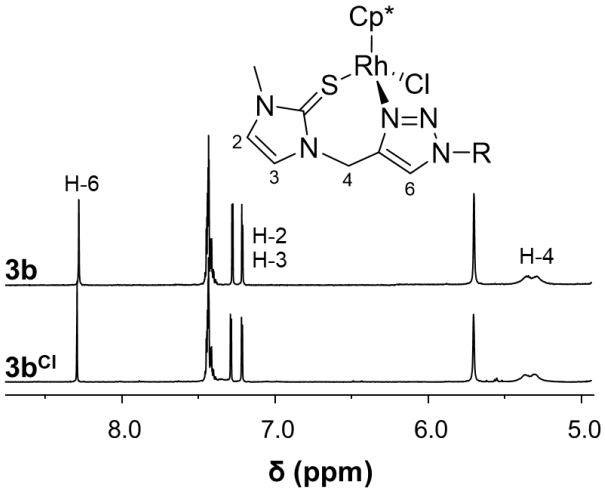

Figure S7. The aromatic regions of the ^{1}H NMR spectra of **3b** and **3b**^{Cl} recorded in MeOD.

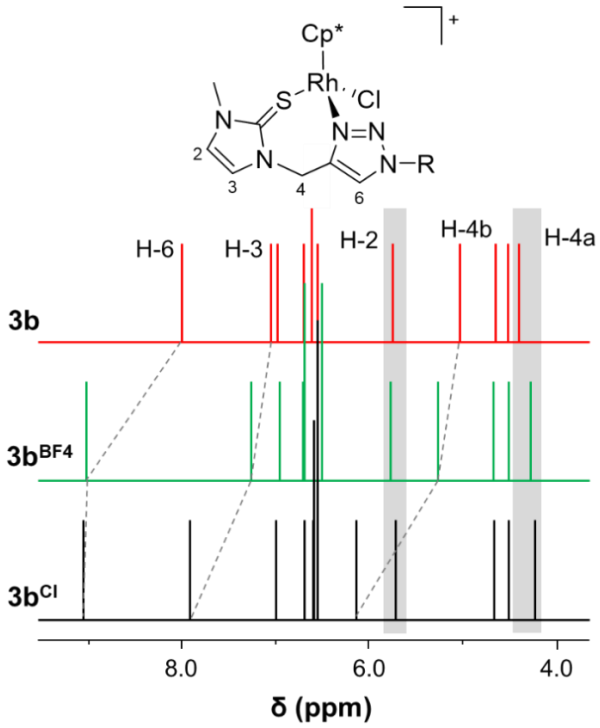

Figure S8. DFT calculations of ^{1}H NMR spectra of **3b**, **3b**^{BF4}, and **3b**^{Cl}.

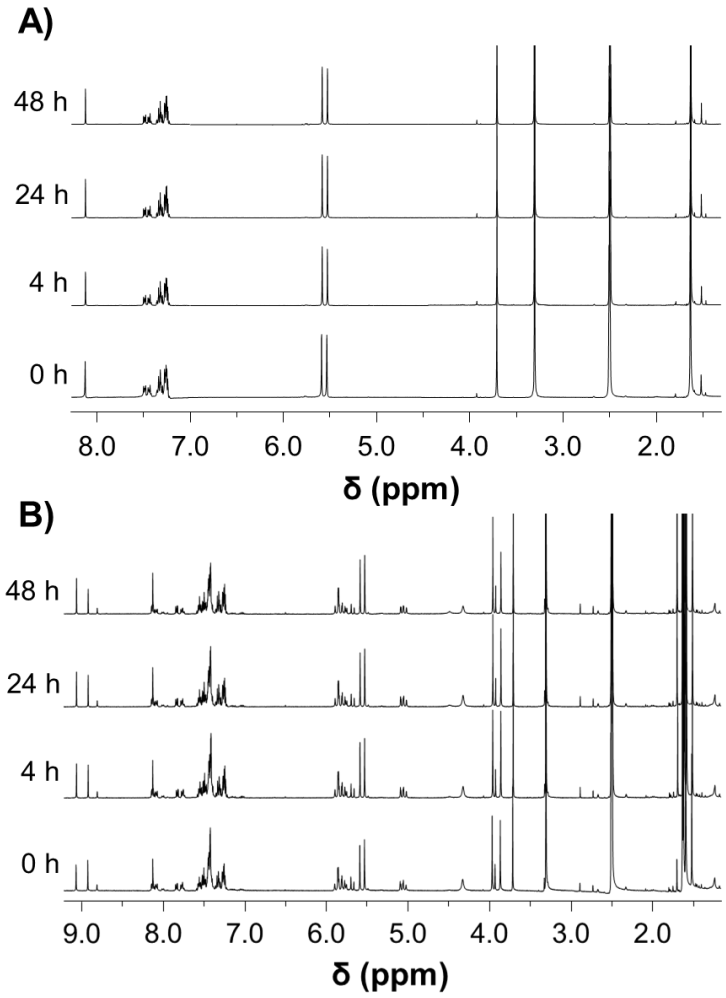

Figure S9. Stability of **4a** (A) and **4a**^{Cl} (B) in DMSO-d_6 investigated by ^{1}H NMR spectroscopy.

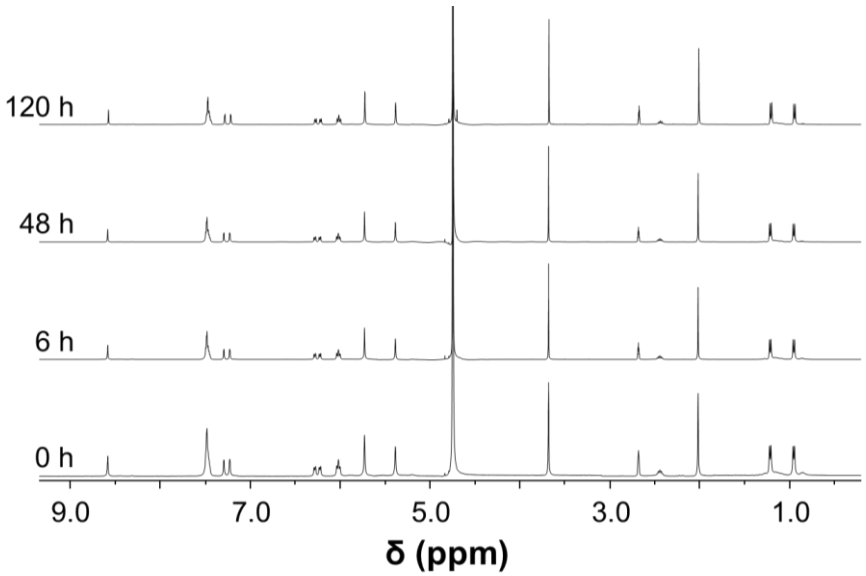

Figure S10. Stability of **1b** in 15% DMSO-d_6/D_2O investigated by ^{1}H NMR spectroscopy.

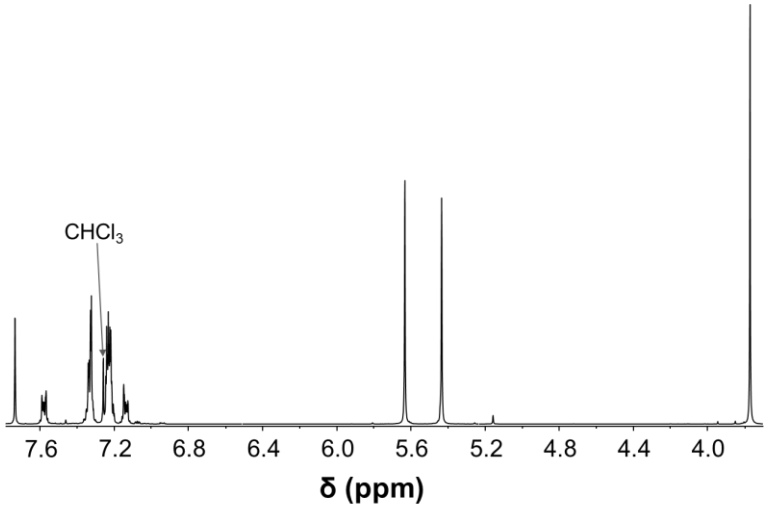

Figure S11. ^{1}H NMR spectrum of 1-[(1-benzyl-1,2,3-triazol-4-yl)methyl]-3-methylbenzimidazole-2-thione **a** recorded in $CDCl_3$.

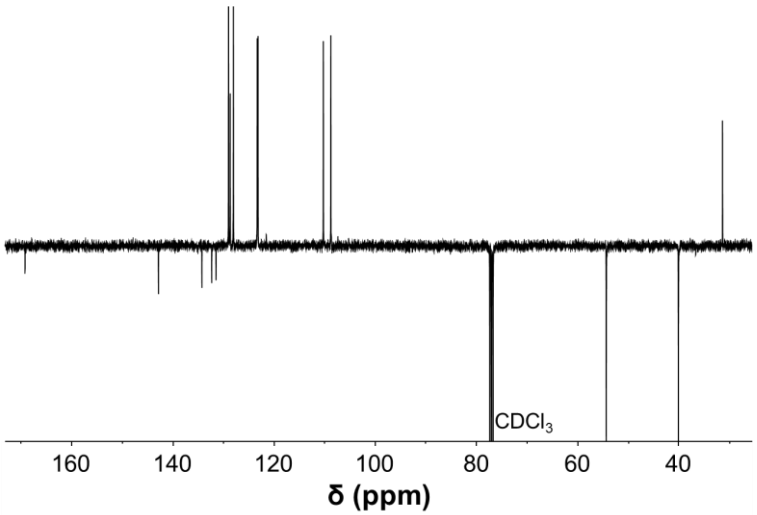

Figure S12. ^{13}C{^{1}H} DEPT-Q NMR spectrum of 1-[(1-benzyl-1,2,3-triazol-4-yl)methyl]-3-methylbenzimidazole-2-thione **a** recorded in $CDCl_3$.

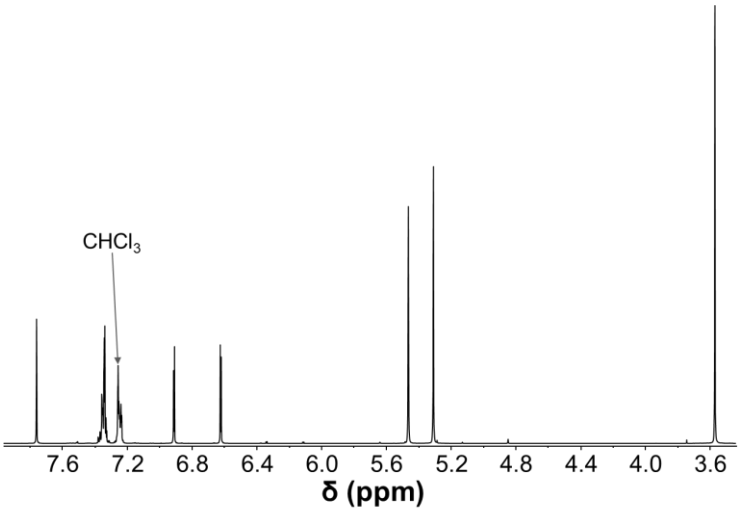

Figure S13. ^{1}H NMR spectrum of 1-[(1-benzyl-1,2,3-triazol-4-yl)methyl]-3-methylimidazole-2-thione **b** recorded in $CDCl_3$.

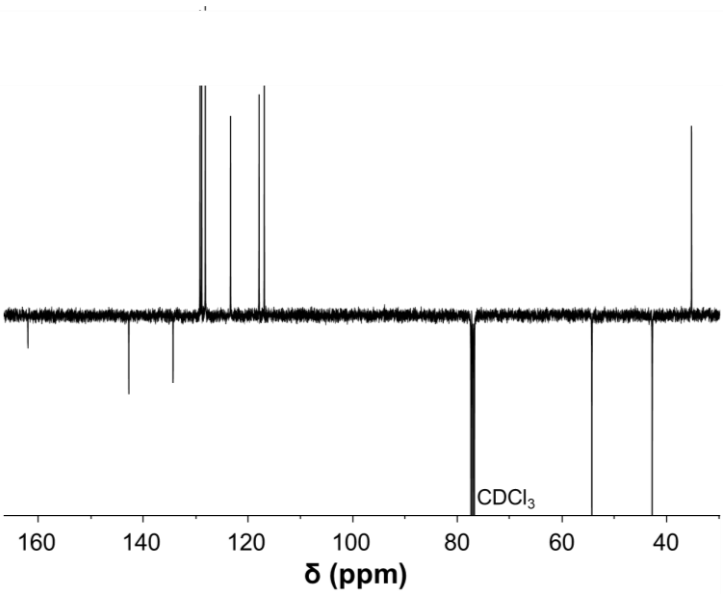

Figure S14. ^{13}C{^{1}H} DEPT-Q NMR spectrum of 1-[(1-benzyl-1,2,3-triazol-4-yl)methyl]-3-methylimidazole-2-thione **b** recorded in $CDCl_3$.

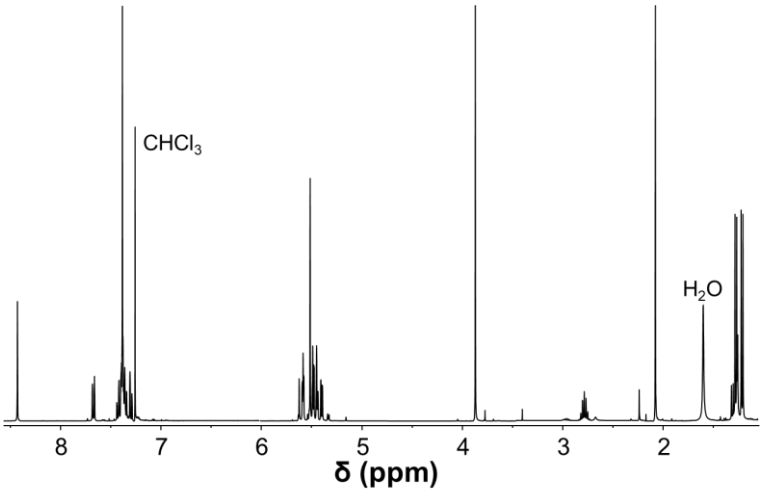

Figure S15. ^{1}H NMR spectrum of [chlorido{1-[(1-benzyl-1,2,3-triazol-4-yl-κ*N*)methyl]-3-methylbenzimidazole-2-thione-κ*S*}(η^{6}-*p*-cymene)ruthenium(II)] hexafluorophosphate **1a** recorded in $CDCl_3$.

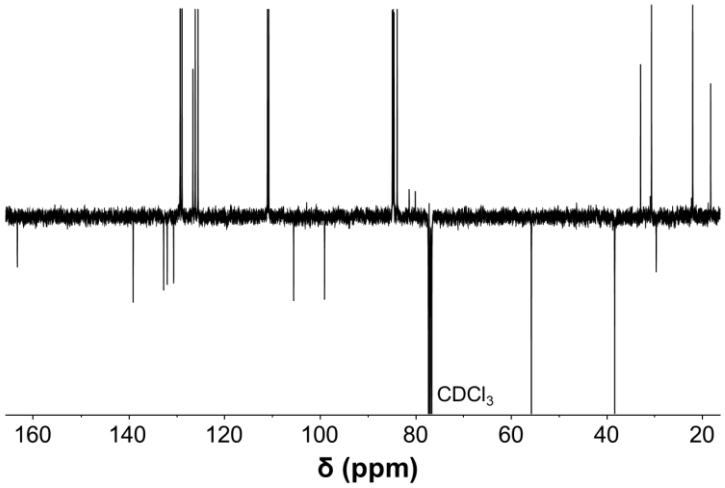

Figure S16. ^{13}C{^{1}H} DEPT-Q NMR spectrum of [chlorido{1-[(1-benzyl-1,2,3-triazol-4-yl-κ*N*)methyl]-3-methylbenzimidazole-2-thione-κ*S*}(η^{6}-*p*-cymene)ruthenium(II)] hexafluorophosphate **1a** recorded in $CDCl_3$.

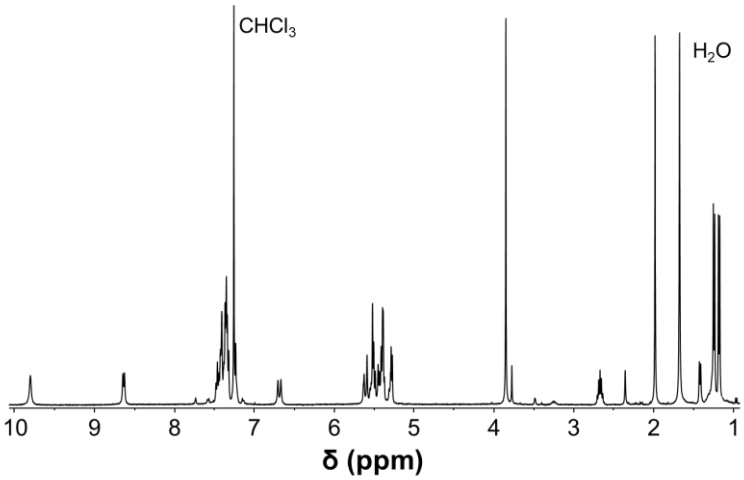

Figure S17. ^{1}H NMR spectrum of [chlorido{1-[(1-benzyl-1,2,3-triazol-4-yl-κ*N*)methyl]-3-methylbenzimidazole-2-thione-κ*S*}(η^{6}-*p*-cymene)ruthenium(II)] chloride **1a**^{Cl} recorded in $CDCl_3$.

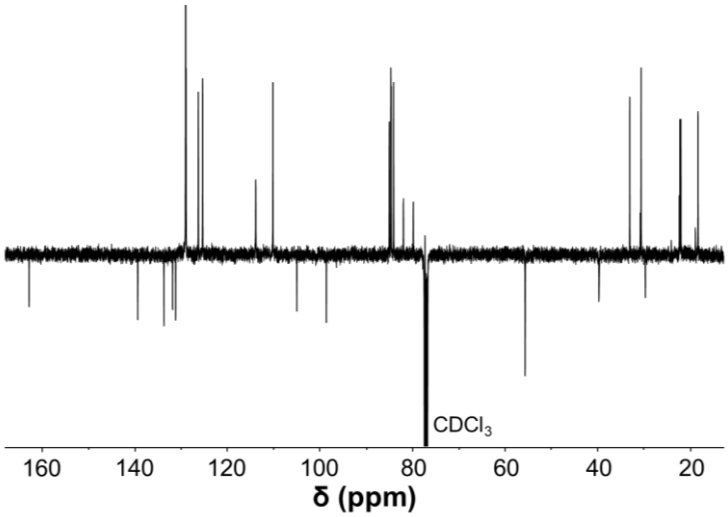

Figure S18. ^{13}C{^{1}H} DEPT-Q NMR spectrum of [chlorido{1-[(1-benzyl-1,2,3-triazol-4-yl-κ*N*)methyl]-3-methylbenzimidazole-2-thione-κ*S*}(η^{6}-*p*-cymene)ruthenium(II)] chloride **1a**^{Cl} recorded in $CDCl_3$.

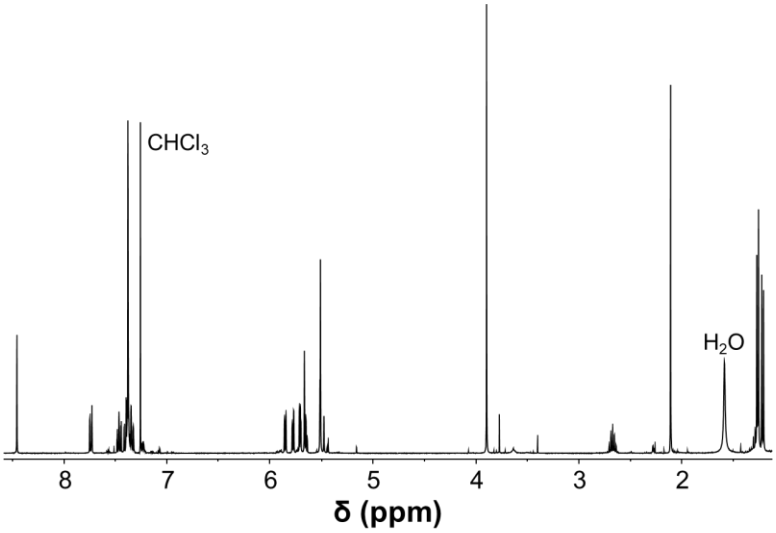

Figure S19. ^{1}H NMR spectrum of [chlorido{1-[(1-benzyl-1,2,3-triazol-4-yl-κ*N*)methyl]-3-methylbenzimidazole-2-thione-κ*S*}(η^{6}-*p*-cymene)osmium(II)] hexafluorophosphate **2a** recorded in $CDCl_3$.

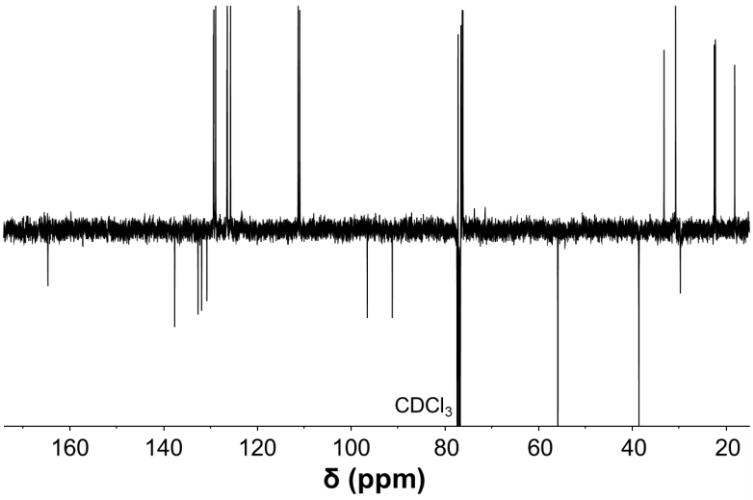

Figure S20. ^{13}C{^{1}H} DEPT-Q NMR spectrum of [chlorido{1-[(1-benzyl-1,2,3-triazol-4-yl-κ*N*)methyl]-3-methylbenzimidazole-2-thione-κ*S*}(η^{6}-*p*-cymene)osmium(II)] hexafluorophosphate **2a** recorded in $CDCl_3$.

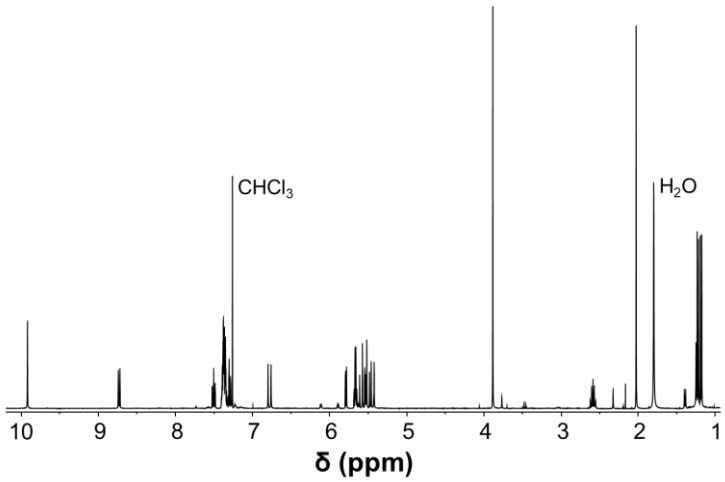

Figure S21. ^{1}H NMR spectrum of [chlorido{1-[(1-benzyl-1,2,3-triazol-4-yl-κN)methyl]-3-methylbenzimidazole-2-thione-κS}(η^{6}-*p*-cymene)osmium(II)] chloride **2a**^{Cl} recorded in $CDCl_3$.

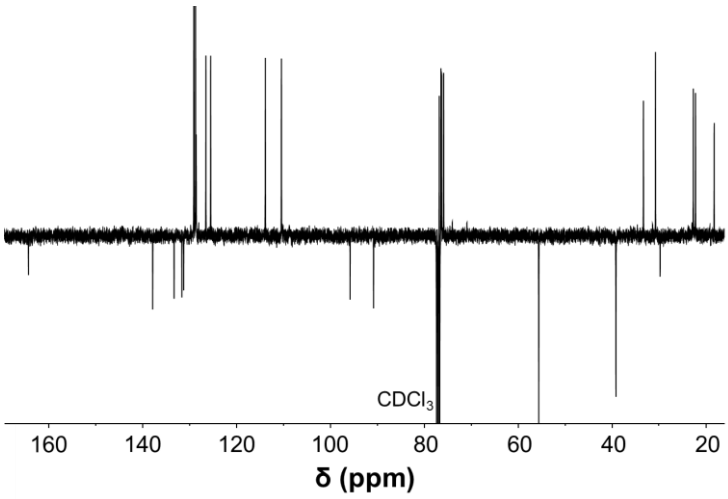

Figure S22. ^{13}C{^{1}H} DEPT-Q NMR spectrum of [chlorido{1-[(1-benzyl-1,2,3-triazol-4-yl-κN)methyl]-3-methylbenzimidazole-2-thione-κS}(η^{6}-*p*-cymene)osmium(II)] chloride **2a**^{Cl} recorded in $CDCl_3$.

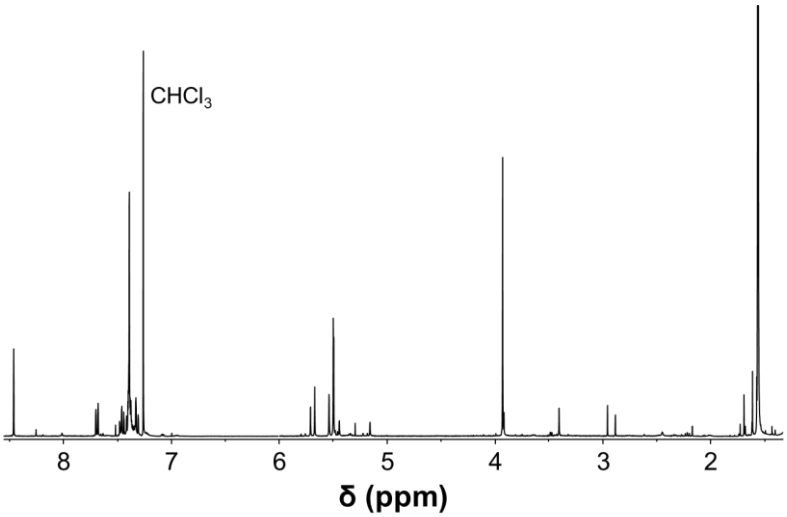

Figure S23. ^{1}H NMR spectrum of [chlorido{1-[(1-benzyl-1,2,3-triazol-4-yl-κN)methyl]-3-methylbenzimidazole-2-thione-κS}(η^{5}-pentamethylcyclopentadiene)rhodium(III)] hexafluorophosphate **3a** recorded in $CDCl_3$.

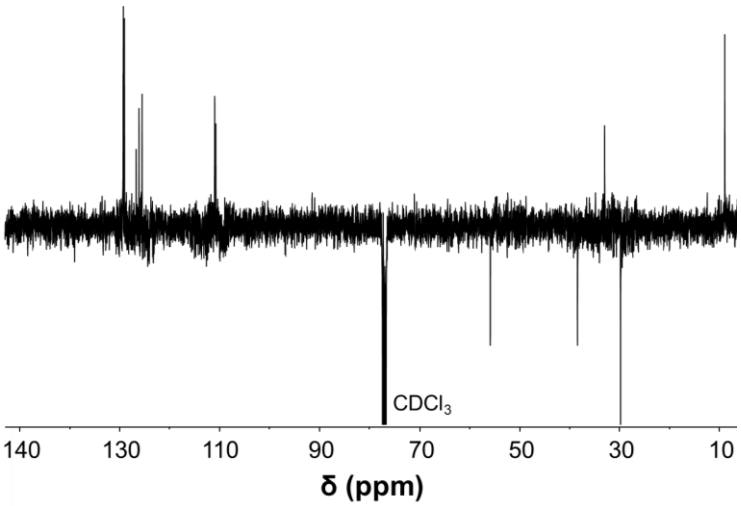

Figure S24. ^{13}C{^{1}H} DEPT-Q NMR spectrum of [chlorido{1-[(1-benzyl-1,2,3-triazol-4-yl-κN)methyl]-3-methylbenzimidazole-2-thione-κS}(η^{5}-pentamethylcyclopentadiene)rhodium(III)] hexafluorophosphate **3a** recorded in $CDCl_3$.

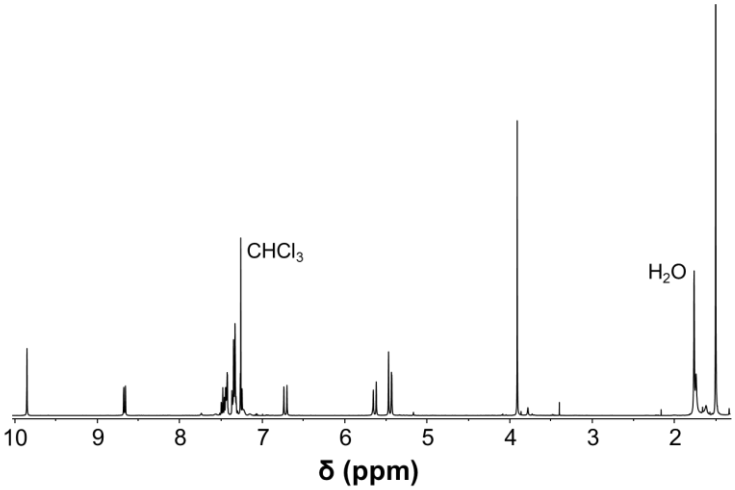

Figure S25. ^{1}H NMR spectrum of [chlorido{1-[(1-benzyl-1,2,3-triazol-4-yl-κN)methyl]-3-methylbenzimidazole-2-thione-κS}(η^{5}-pentamethylcyclopentadiene)rhodium(III)] chloride **3a**^{Cl} recorded in $CDCl_3$.

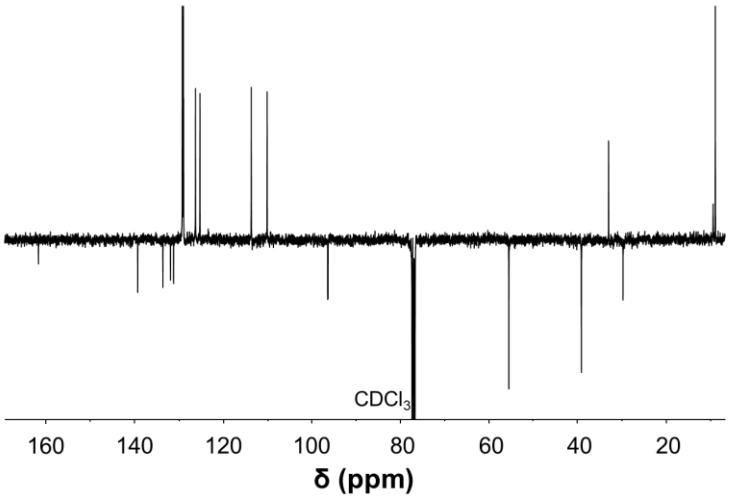

Figure S26. ^{13}C{^{1}H} DEPT-Q NMR spectrum of [chlorido{1-[(1-benzyl-1,2,3-triazol-4-yl-κN)methyl]-3-methylbenzimidazole-2-thione-κS}(η^{5}-pentamethylcyclopentadiene)rhodium(III)] chloride **3a**^{Cl} recorded in $CDCl_3$.

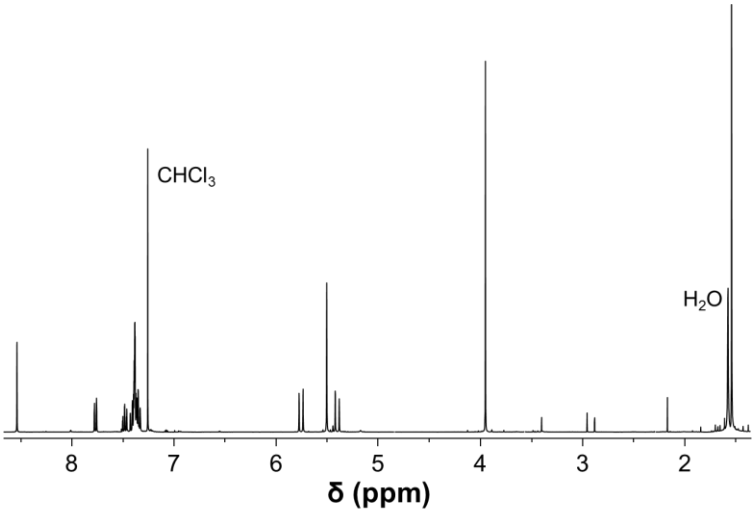

Figure S27. ^{1}H NMR spectrum of [chlorido{1-[(1-benzyl-1,2,3-triazol-4-yl-κN)methyl]-3-methylbenzimidazole-2-thione-κS}(η^{5}-pentamethylcyclopentadiene)iridium(III)] hexafluorophosphate **4a** recorded in $CDCl_3$.

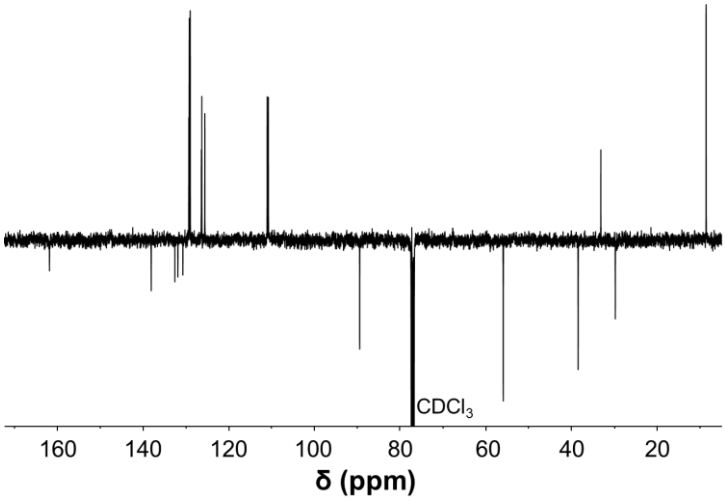

Figure S28. ^{13}C{^{1}H} DEPT-Q NMR spectrum of [chlorido{1-[(1-benzyl-1,2,3-triazol-4-yl-κN)methyl]-3-methylbenzimidazole-2-thione-κS}(η^{5}-pentamethylcyclopentadiene)iridium(III)] hexafluorophosphate **4a** recorded in $CDCl_3$.

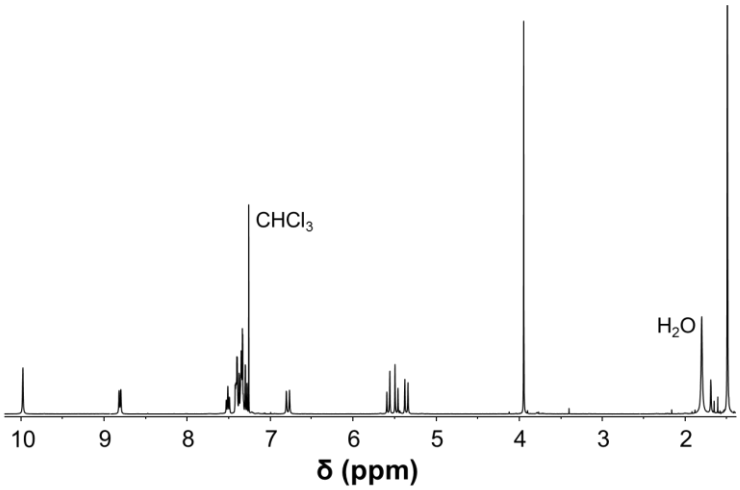

Figure S29. ^{1}H NMR spectrum of [chlorido{1-[(1-benzyl-1,2,3-triazol-4-yl-κN)methyl]-3-methylbenzimidazole-2-thione-κS}(η^{5}-pentamethylcyclopentadiene)iridium(III)] chloride **4a**^{Cl} recorded in $CDCl_3$.

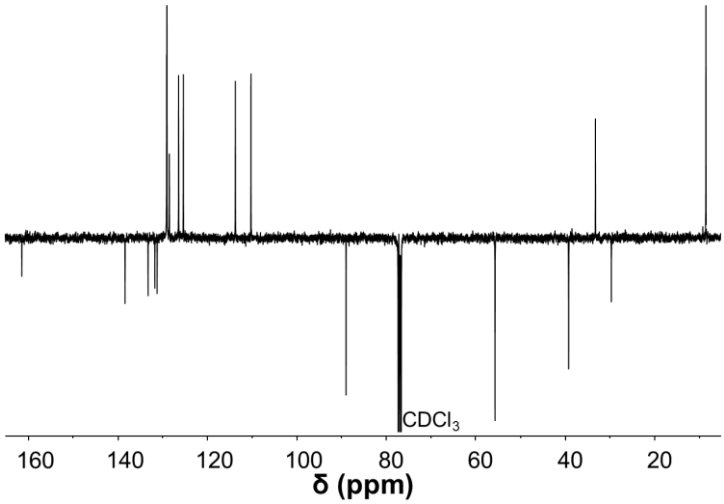

Figure S30. ^{13}C{^{1}H} DEPT-Q NMR spectrum of [chlorido{1-[(1-benzyl-1,2,3-triazol-4-yl-κN)methyl]-3-methylbenzimidazole-2-thione-κS}(η^{5}-pentamethylcyclopentadiene)iridium(III)] chloride **4a**^{Cl} recorded in $CDCl_3$.

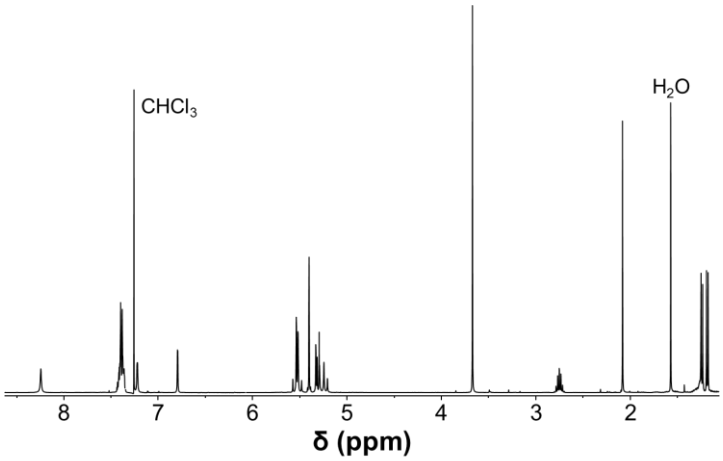

Figure S31. ^{1}H NMR spectrum of [chlorido{1-[(1-benzyl-1,2,3-triazol-4-yl-κN)methyl]-3-methylimidazole-2-thione-κS}(η^{6}-*p*-cymene)ruthenium(II)] hexafluorophosphate **1b** recorded in $CDCl_3$.

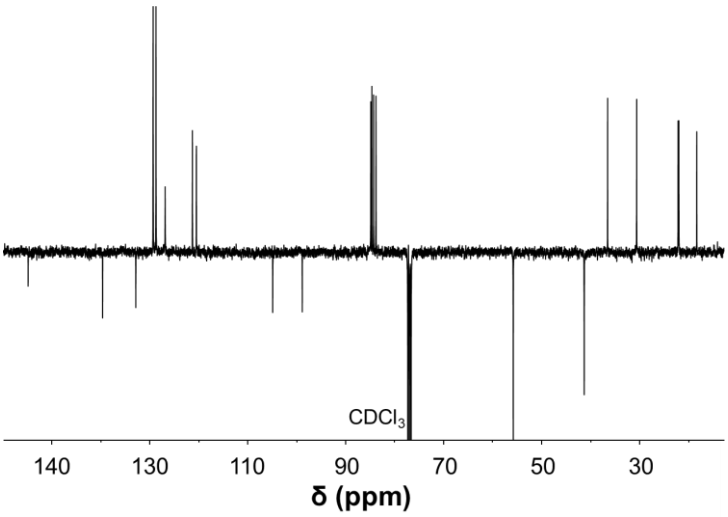

Figure S32. ^{13}C{^{1}H} DEPT-Q NMR spectrum of [chlorido{1-[(1-benzyl-1,2,3-triazol-4-yl-κN)methyl]-3-methylimidazole-2-thione-κS}(η^{6}-*p*-cymene)ruthenium(II)] hexafluorophosphate **1b** recorded in $CDCl_3$.

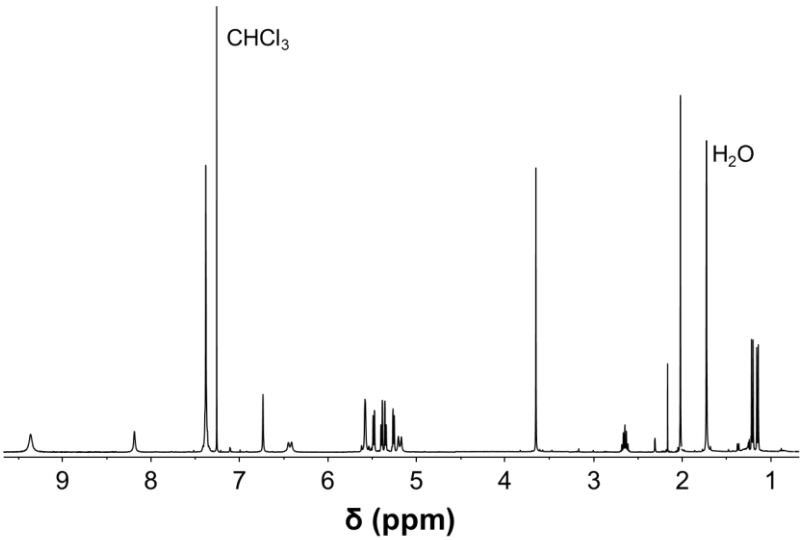

Figure S33. ^{1}H NMR spectrum of [chlorido{1-[(1-benzyl-1,2,3-triazol-4-yl-κN)methyl]-3-methylimidazole-2-thione-κS}(η^{6}-*p*-cymene)ruthenium(II)] chloride **1b^{Cl}** recorded in $CDCl_3$.

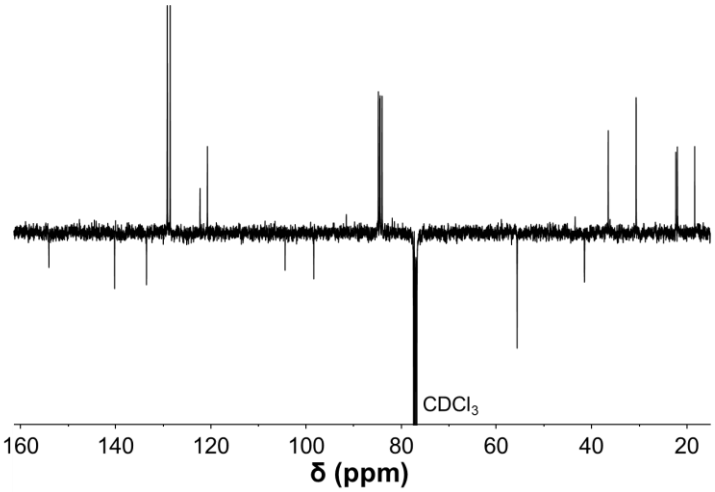

Figure S34. ^{13}C{^{1}H} DEPT-Q NMR spectrum of [chlorido{1-[(1-benzyl-1,2,3-triazol-4-yl-κN)methyl]-3-methylimidazole-2-thione-κS}(η^{6}-*p*-cymene)ruthenium(II)] chloride **1b^{Cl}** recorded in $CDCl_3$.

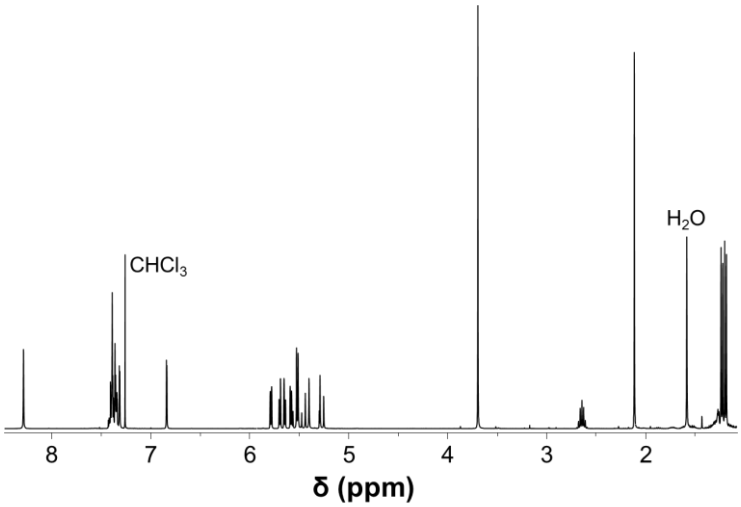

Figure S35. ^{1}H NMR spectrum of [chlorido{1-[(1-benzyl-1,2,3-triazol-4-yl-κN)methyl]-3-methylimidazole-2-thione-κS}(η^{6}-*p*-cymene)osmium(II)] hexafluorophosphate **2b** recorded in $CDCl_3$.

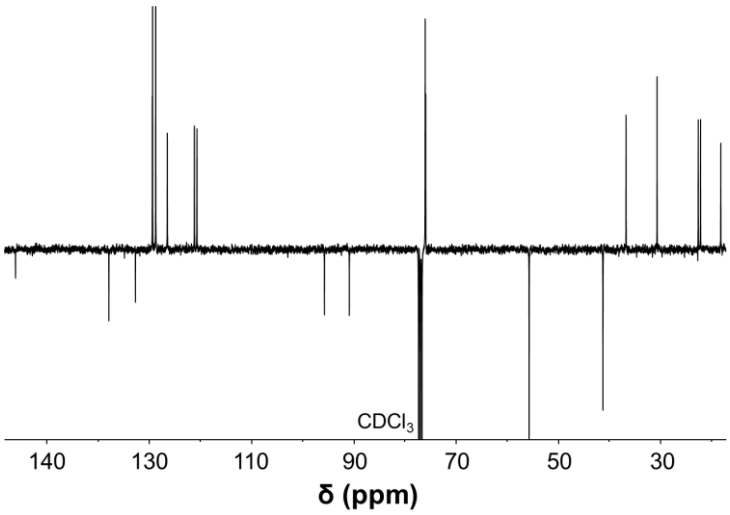

Figure S36. ^{13}C{^{1}H} DEPT-Q NMR spectrum of [chlorido{1-[(1-benzyl-1,2,3-triazol-4-yl-κN)methyl]-3-methylimidazole-2-thione-κS}(η^{6}-*p*-cymene)osmium(II)] hexafluorophosphate **2b** recorded in $CDCl_3$.

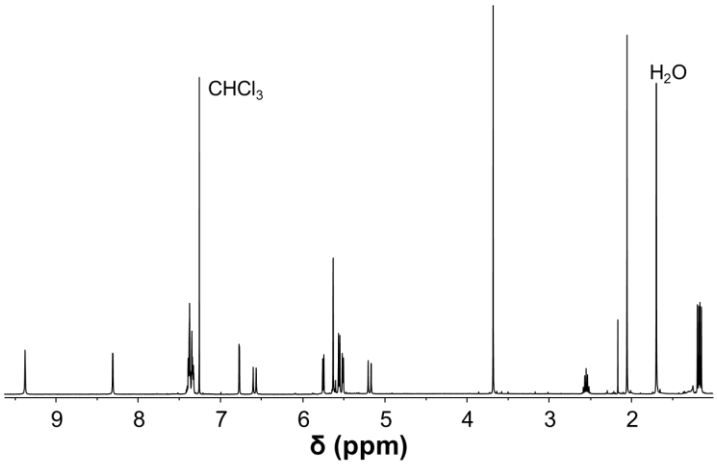

Figure S37. ^{1}H NMR spectrum of [chlorido{1-[(1-benzyl-1,2,3-triazol-4-yl-κN)methyl]-3-methylimidazole-2-thione-κS}(η^{6}-*p*-cymene)osmium(II)] chloride **2b^{Cl}** recorded in $CDCl_3$.

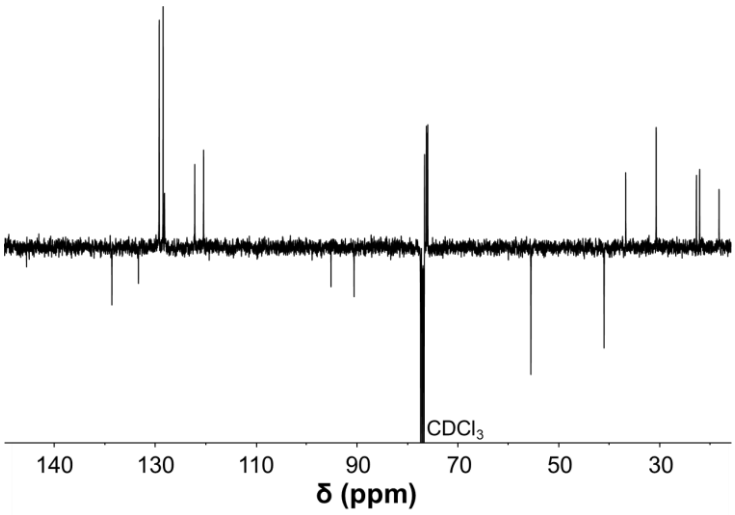

Figure S38. ^{13}C{^{1}H} DEPT-Q NMR spectrum of [chlorido{1-[(1-benzyl-1,2,3-triazol-4-yl-κN)methyl]-3-methylimidazole-2-thione-κS}(η^{6}-*p*-cymene)osmium(II)] chloride **2b^{Cl}** recorded in $CDCl_3$.

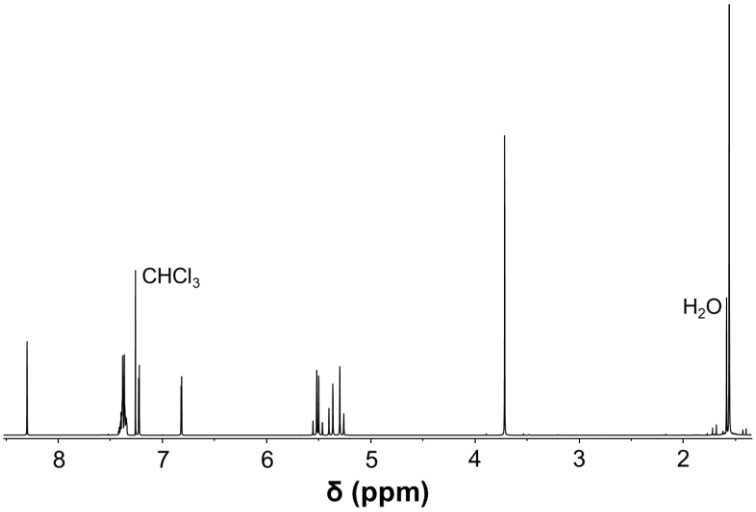

Figure S39. ^{1}H NMR spectrum of [chlorido{1-[(1-benzyl-1,2,3-triazol-4-yl-κN)methyl]-3-methylimidazole-2-thione-κS}(η^{5}-pentamethylcyclopentadiene)rhodium(III)] hexafluorophosphate **3b** recorded in $CDCl_3$.

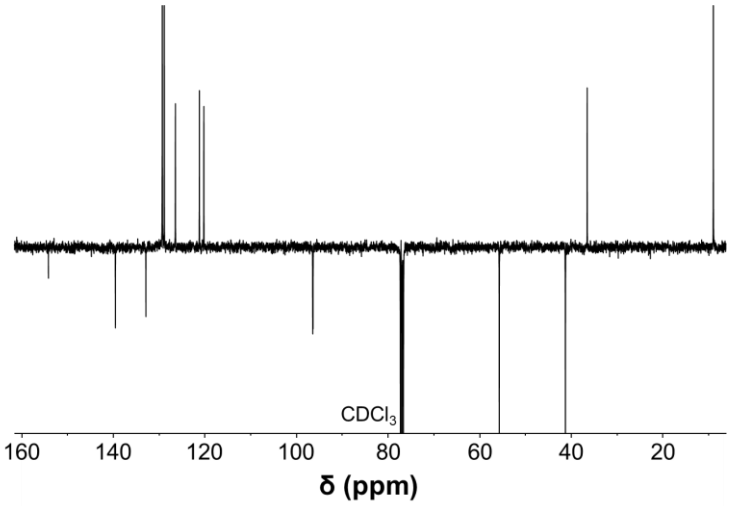

Figure S40. ^{13}C{^{1}H} DEPT-Q NMR spectrum of [chlorido{1-[(1-benzyl-1,2,3-triazol-4-yl-κN)methyl]-3-methylimidazole-2-thione-κS}(η^{5}-pentamethylcyclopentadiene)rhodium(III)] hexafluorophosphate **3b** recorded in $CDCl_3$.

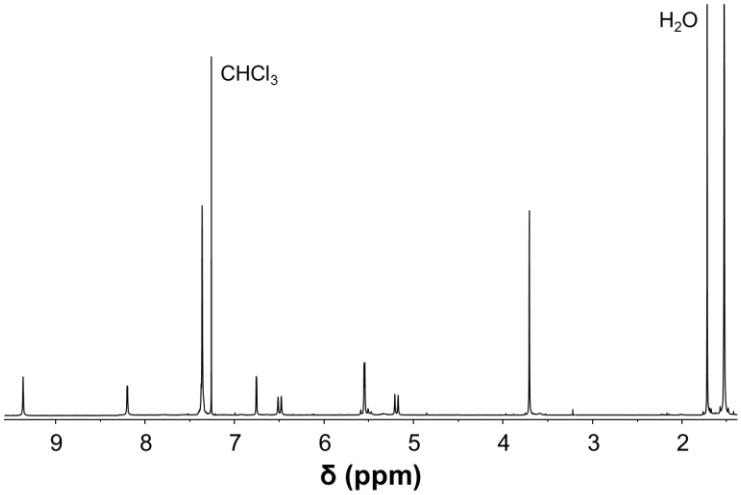

Figure S41. ^{1}H NMR spectrum of [chlorido{1-[(1-benzyl-1,2,3-triazol-4-yl-κN)methyl]-3-methylimidazole-2-thione-κS}(η^{5}-pentamethylcyclopentadiene)rhodium(III)] chloride **3b**^{Cl} recorded in $CDCl_3$.

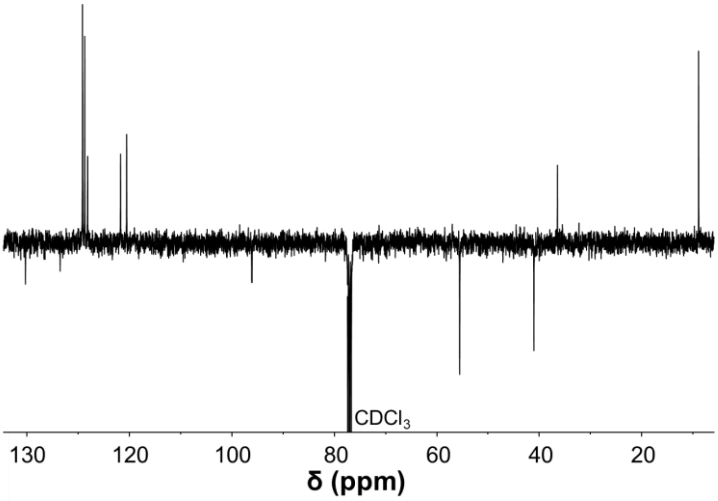

Figure S42. ^{13}C{^{1}H} DEPT-Q NMR spectrum of [chlorido{1-[(1-benzyl-1,2,3-triazol-4-yl-κN)methyl]-3-methylimidazole-2-thione-κS}(η^{5}-pentamethylcyclopentadiene)rhodium(III)] chloride **3b**^{Cl} recorded in $CDCl_3$.

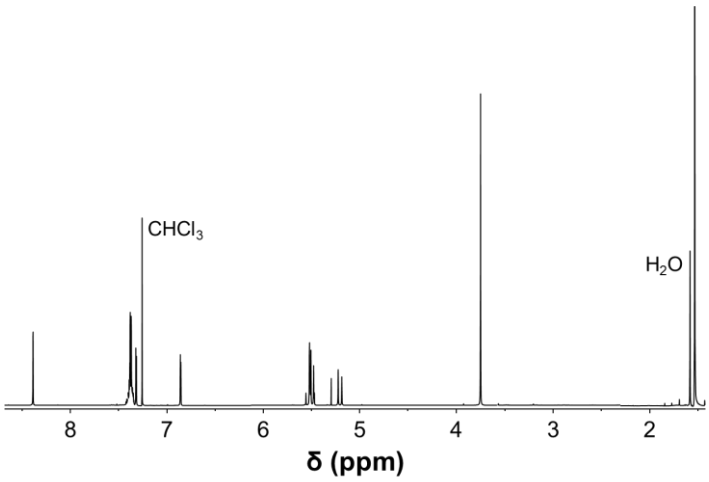

Figure S43. ^{1}H NMR spectrum of [chlorido{1-[(1-benzyl-1,2,3-triazol-4-yl-κN)methyl]-3-methylimidazole-2-thione-κS}(η^{5}-pentamethylcyclopentadiene)iridium(III)] hexafluorophosphate **4b** recorded in $CDCl_3$.

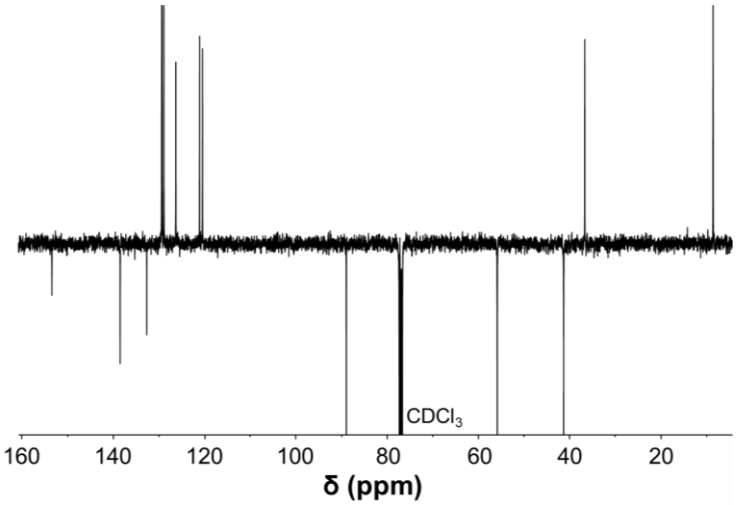

Figure S44. ^{13}C{^{1}H} DEPT-Q NMR spectrum of [chlorido{1-[(1-benzyl-1,2,3-triazol-4-yl-κN)methyl]-3-methylimidazole-2-thione-κS}(η^{5}-pentamethylcyclopentadiene)iridium(III)] hexafluorophosphate **4b** recorded in $CDCl_3$.

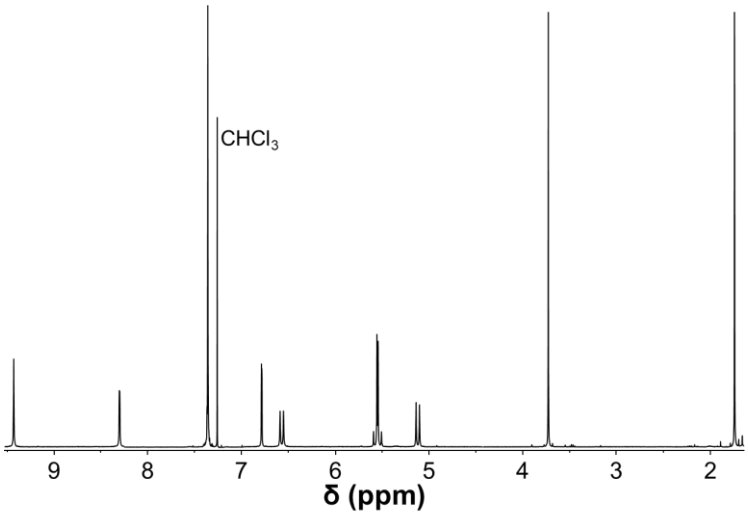

Figure S45. ^{1}H NMR spectrum of [chlorido{1-[(1-benzyl-1,2,3-triazol-4-yl-κN)methyl]-3-methylimidazole-2-thione-κS}(η^{5}-pentamethylcyclopentadiene)iridium(III)] chloride **4b^{Cl}** recorded in $CDCl_3$.

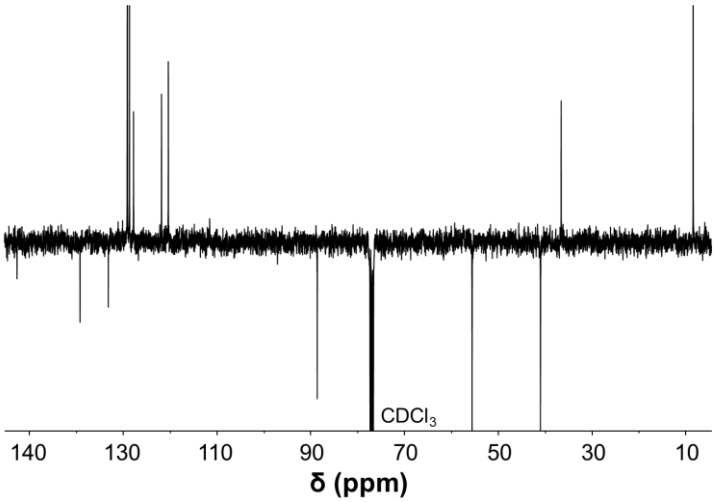

Figure S46. ^{13}C{^{1}H} DEPT-Q NMR spectrum of [chlorido{1-[(1-benzyl-1,2,3-triazol-4-yl-κN)methyl]-3-methylimidazole-2-thione-κS}(η^{5}-pentamethylcyclopentadiene)iridium(III)] chloride **4b^{Cl}** recorded in $CDCl_3$.

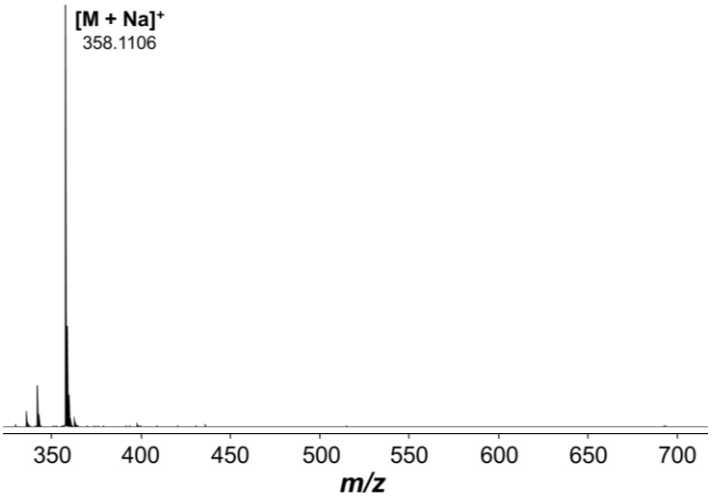

Figure S47. Electrospray ionization mass spectrum of 1-[(1-benzyl-1,2,3-triazol-4-yl)methyl]-3-methylbenzimidazole-2-thione **a**.

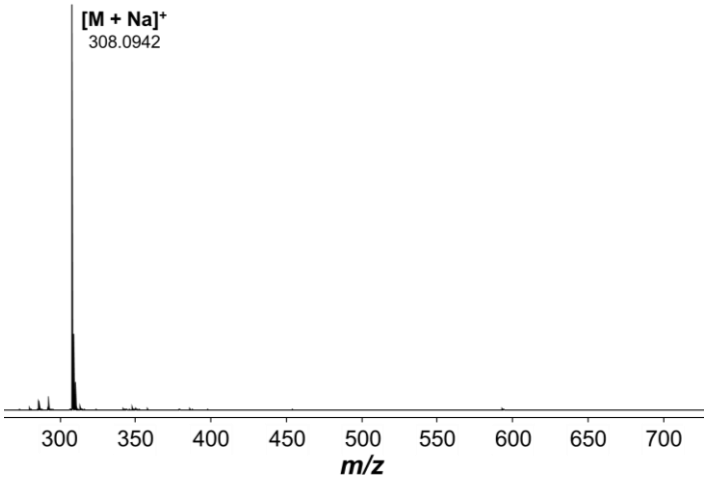

Figure S48. Electrospray ionization mass spectrum of 1-[(1-benzyl-1,2,3-triazol-4-yl)methyl]-3-methylimidazole-2-thione **b**.

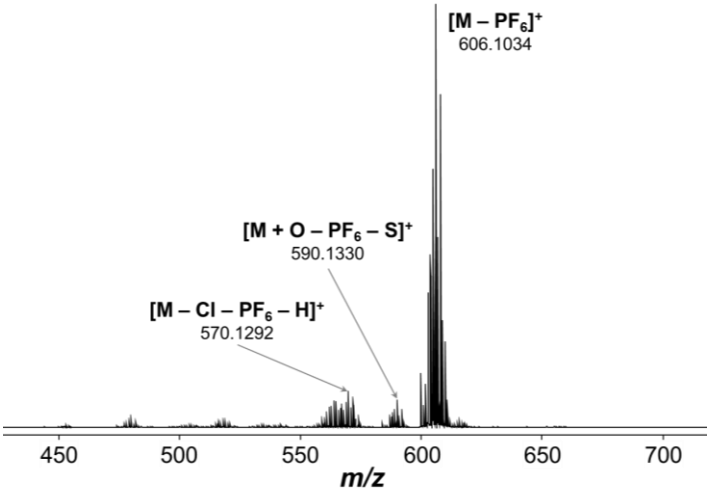

Figure S49. Electrospray ionization mass spectrum of [chlorido{1-[(1-benzyl-1,2,3-triazol-4-yl-κ*N*)methyl]-3-methylbenzimidazole-2-thione-κ*S*}(η^6-*p*-cymene)ruthenium(II)] hexafluorophosphate **1a**.

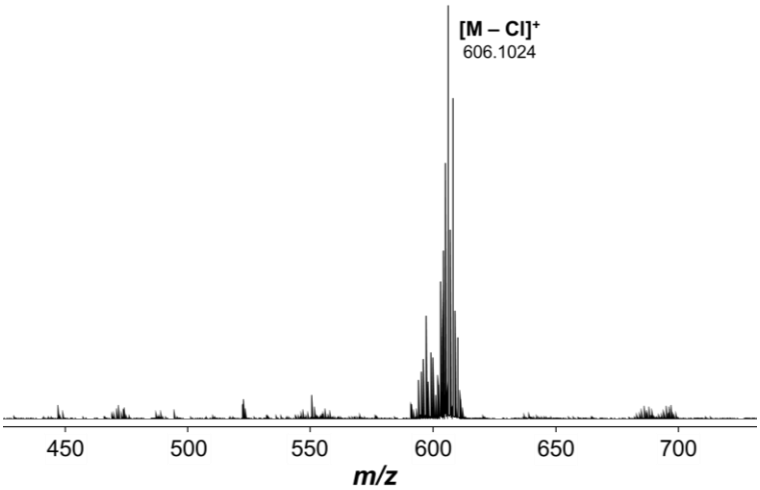

Figure S50. Electrospray ionization mass spectrum of [chlorido{1-[(1-benzyl-1,2,3-triazol-4-yl-κ*N*)methyl]-3-methylbenzimidazole-2-thione-κ*S*}(η^6-*p*-cymene)ruthenium(II)] chloride **1a**^{Cl}.

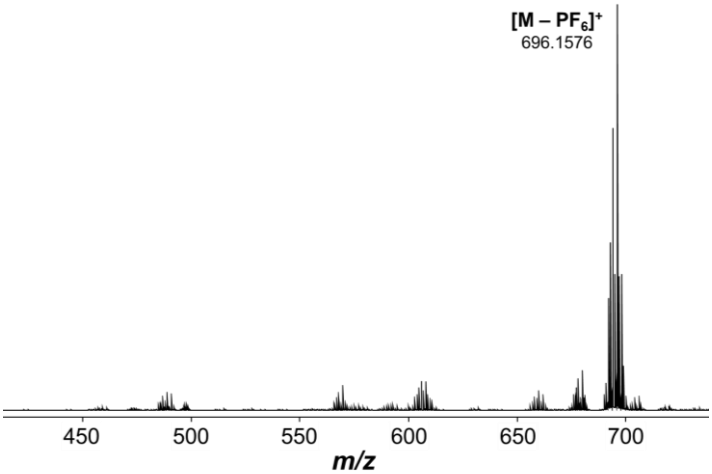

Figure S51. Electrospray ionization mass spectrum of [chlorido{1-[(1-benzyl-1,2,3-triazol-4-yl-κ*N*)methyl]-3-methylbenzimidazole-2-thione-κ*S*}(η^6-*p*-cymene)osmium(II)] hexafluorophosphate **2a**.

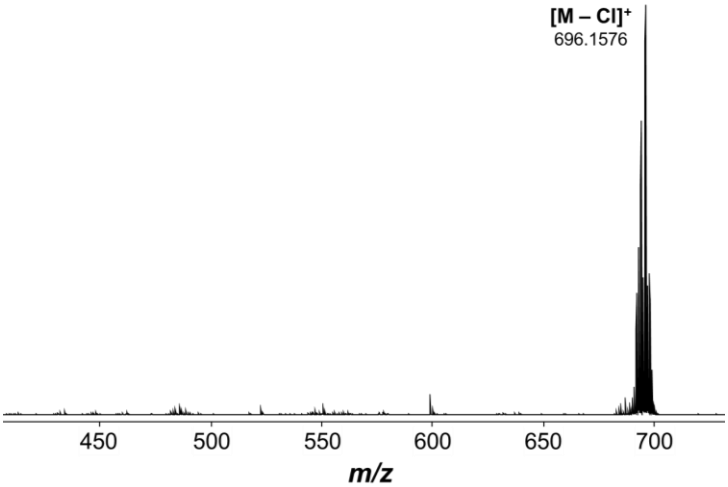

Figure S52. Electrospray ionization mass spectrum of [chlorido{1-[(1-benzyl-1,2,3-triazol-4-yl-κN)methyl]-3-methylbenzimidazole-2-thione-κS}(η^6-*p*-cymene)osmium(II)] chloride **2a**^{Cl}.

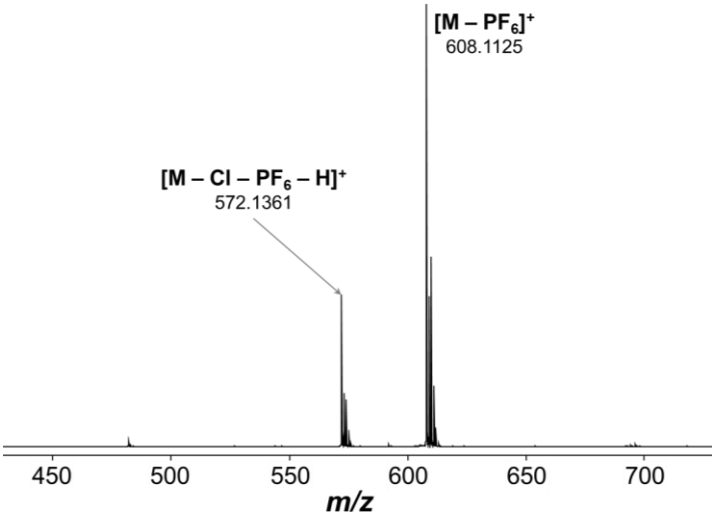

Figure S53. Electrospray ionization mass spectrum of [chlorido{1-[(1-benzyl-1,2,3-triazol-4-yl-κN)methyl]-3-methylbenzimidazole-2-thione-κS}(η^5-pentamethylcyclopentadiene)rhodium(III)] hexafluorophosphate **3a**.

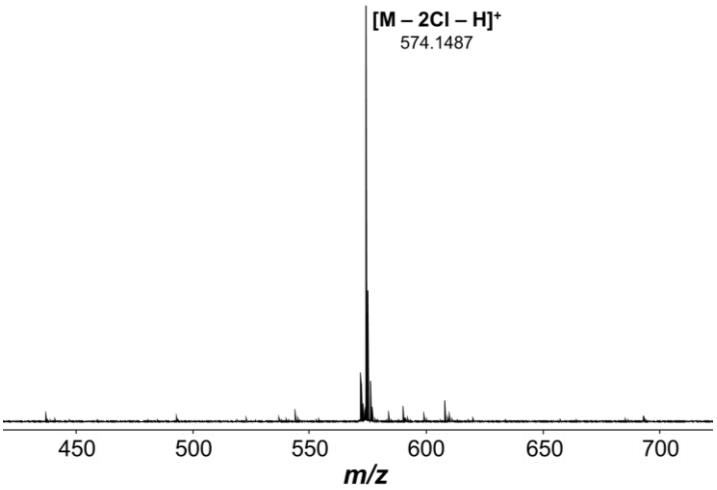

Figure S54. Electrospray ionization mass spectrum of [chlorido{1-[(1-benzyl-1,2,3-triazol-4-yl-κN)methyl]-3-methylbenzimidazole-2-thione-κS}(η^5-pentamethylcyclopentadiene)rhodium(III)] chloride **3a**^{Cl}.

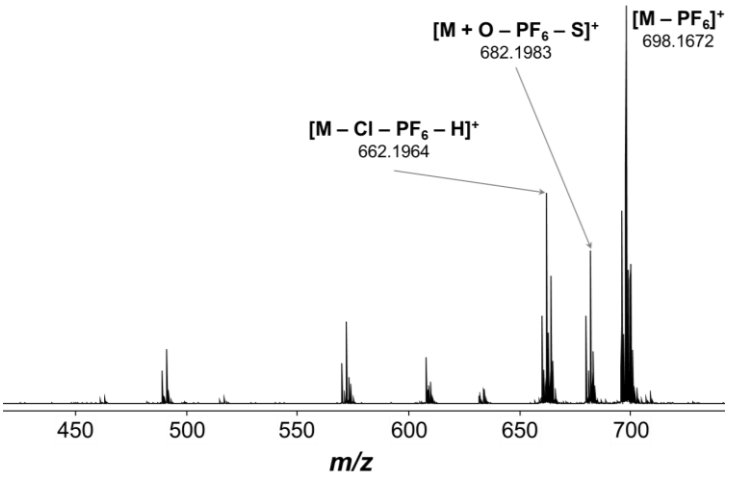

Figure S55. Electrospray ionization mass spectrum of [chlorido{1-[(1-benzyl-1,2,3-triazol-4-yl-κN)methyl]-3-methylbenzimidazole-2-thione-κS}(η^5-pentamethylcyclopentadiene)iridium(III)] hexafluorophosphate **4a**.

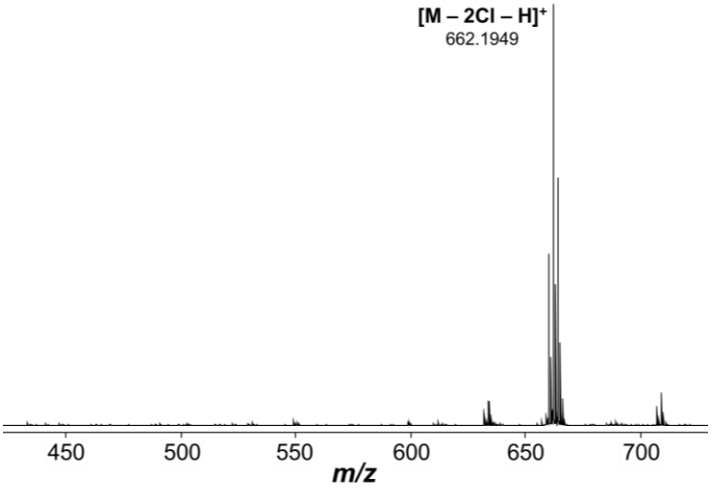

Figure S56. Electrospray ionization mass spectrum of [chlorido{1-[(1-benzyl-1,2,3-triazol-4-yl-κN)methyl]-3-methylbenzimidazole-2-thione-κS}(η^5-pentamethylcyclopentadiene)iridium(III)] chloride **4a**^{Cl}.

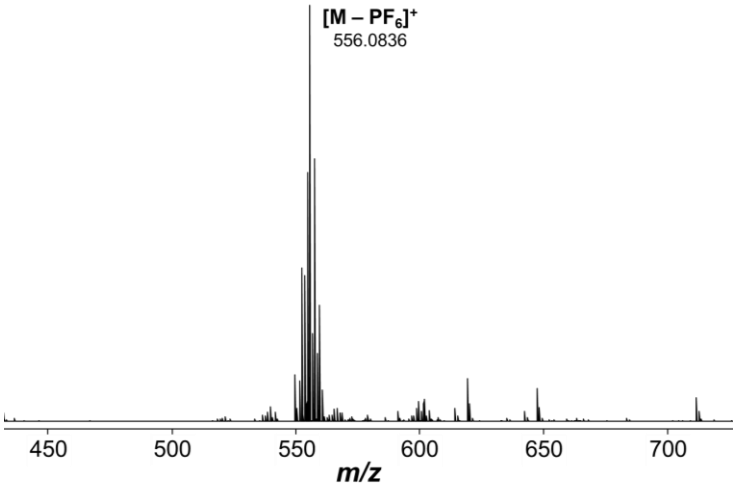

Figure S57. Electrospray ionization mass spectrum of [chlorido{1-[(1-benzyl-1,2,3-triazol-4-yl-κN)methyl]-3-methylimidazole-2-thione-κS}(η^6-*p*-cymene)ruthenium(II)] hexafluorophosphate **1b**.

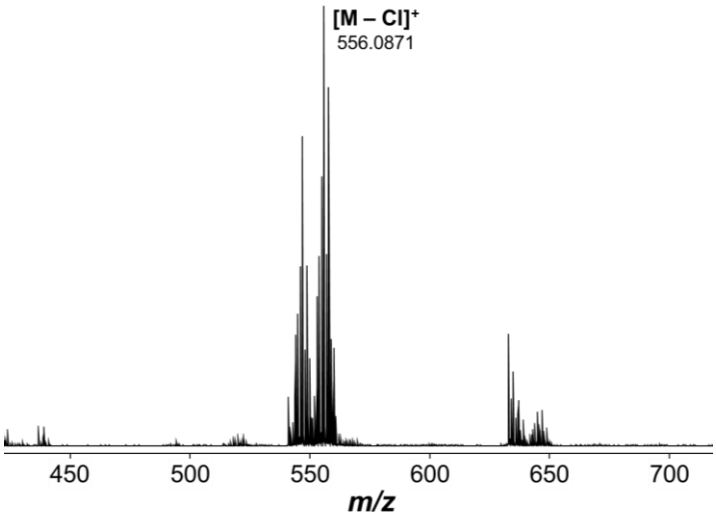

Figure S58. Electrospray ionization mass spectrum of [chlorido{1-[(1-benzyl-1,2,3-triazol-4-yl-κN)methyl]-3-methylimidazole-2-thione-κS}(η^6-*p*-cymene)ruthenium(II)] chloride **1b**^{Cl}.

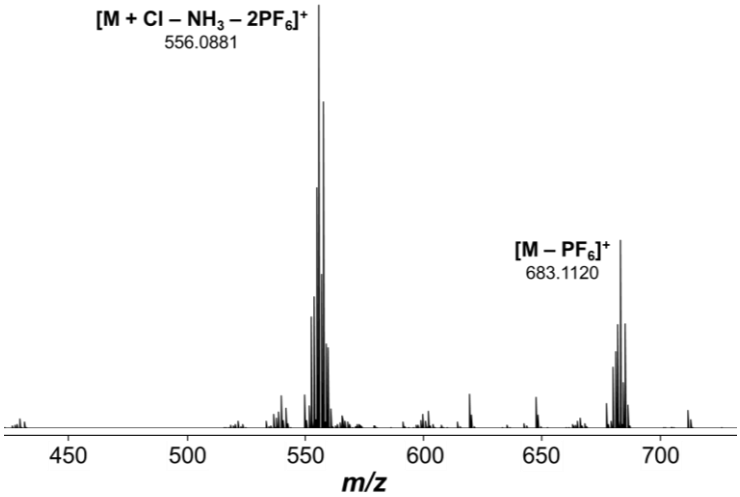

Figure S59. Electrospray ionization mass spectrum of [ammine{1-[(1-benzyl-1,2,3-triazol-4-yl-κN)methyl]-3-methylimidazole-2-thione-κS}(η^6-*p*-cymene)ruthenium(II)] hexafluorophosphate **1b**^{NH3}.

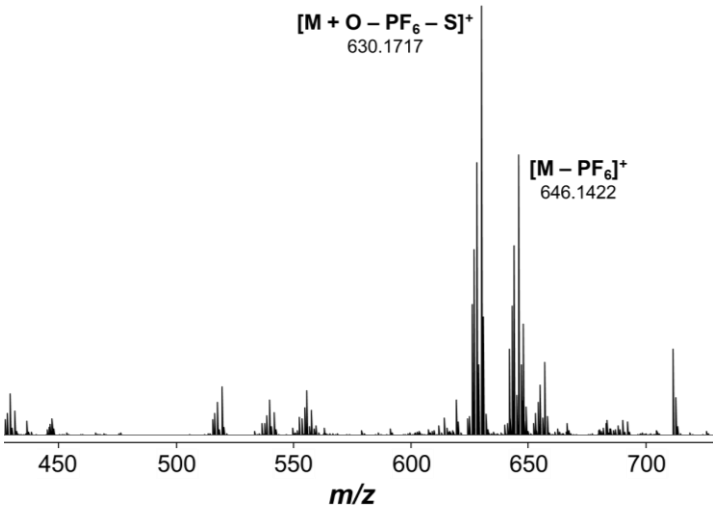

Figure S60. Electrospray ionization mass spectrum of [chlorido{1-[(1-benzyl-1,2,3-triazol-4-yl-κN)methyl]-3-methylimidazole-2-thione-κS}(η^6-*p*-cymene)osmium(II)] hexafluorophosphate **2b**.

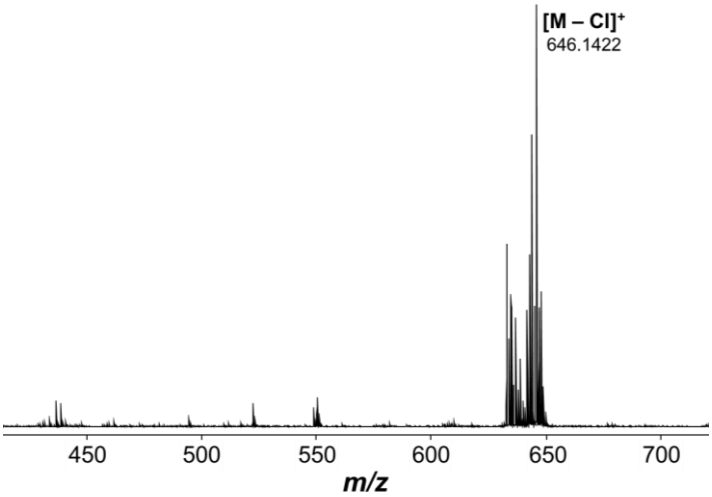

Figure S61. Electrospray ionization mass spectrum of [chlorido{1-[(1-benzyl-1,2,3-triazol-4-yl-κN)methyl]-3-methylimidazole-2-thione-κS}(η^6-*p*-cymene)osmium(II)] chloride **2b**^{Cl}.

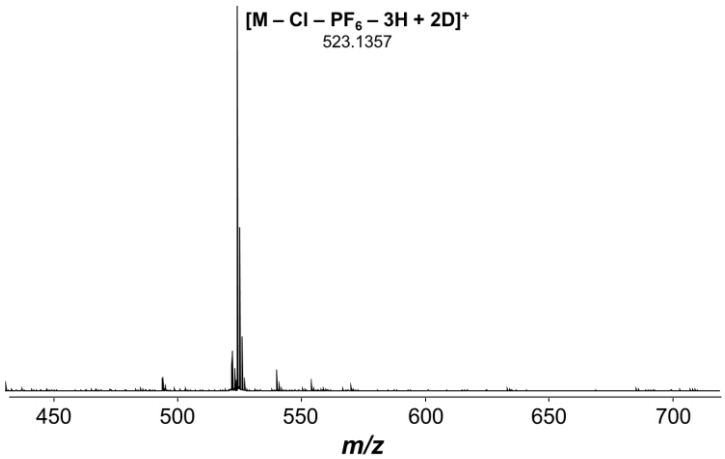

Figure S62. Electrospray ionization mass spectrum of [chlorido{1-[(1-benzyl-1,2,3-triazol-4-yl-κN)methyl]-3-methylimidazole-2-thione-κS}(η^5-pentamethylcyclopentadiene)rhodium(III)] hexafluorophosphate **3b**.

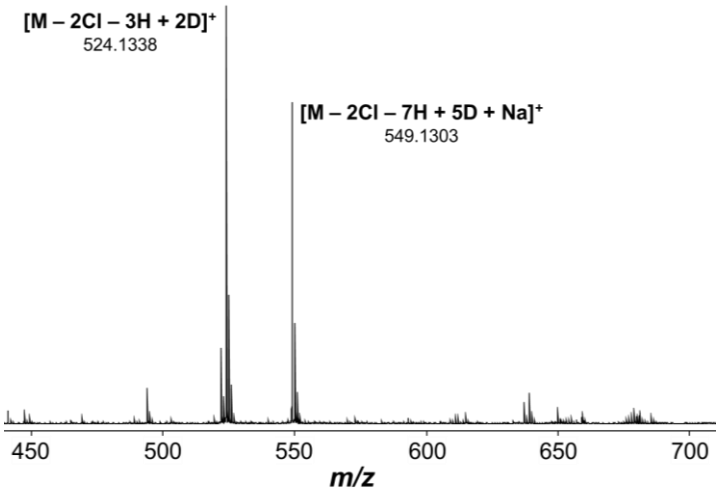

Figure S63. Electrospray ionization mass spectrum of [chlorido{1-[(1-benzyl-1,2,3-triazol-4-yl-κN)methyl]-3-methylimidazole-2-thione-κS}(η^5-pentamethylcyclopentadiene)rhodium(III)] chloride **3b**^{Cl}.

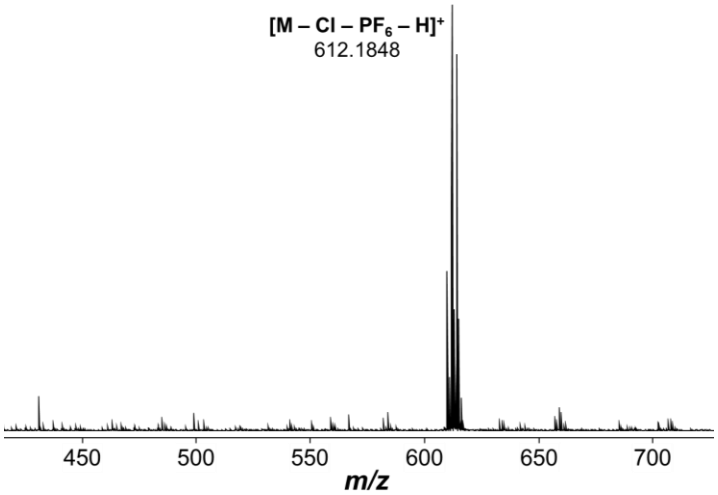

Figure S64. Electrospray ionization mass spectrum of [chlorido{1-[(1-benzyl-1,2,3-triazol-4-yl-κN)methyl]-3-methylimidazole-2-thione-κS}(η^5-pentamethylcyclopentadiene)iridium(III)] hexafluorophosphate **4b**.

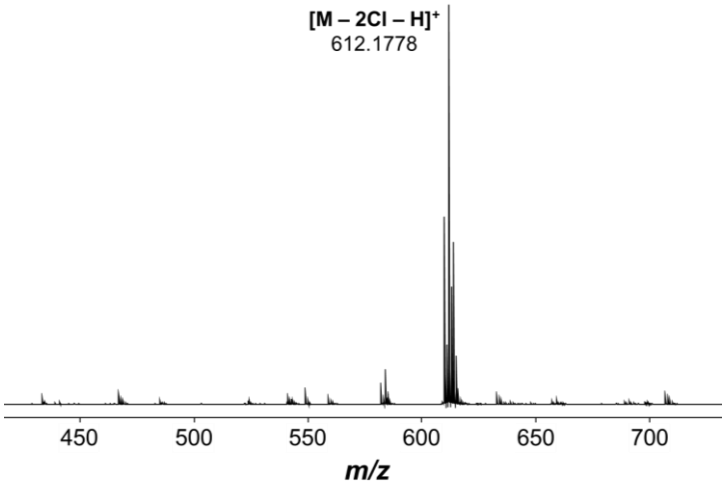

Figure S65. Electrospray ionization mass spectrum of [chlorido{1-[(1-benzyl-1,2,3-triazol-4-yl-κN)methyl]-3-methylimidazole-2-thione-κS}(η^5-pentamethylcyclopentadiene)iridium(III)] chloride **4b**^{Cl}.